Tetranuclear Tetrapyrido[3,2-a:2′,3′-c:3″,2″-h:2‴,3‴-j]phenazineruthenium Complex: Synthesis, Wide-Angle X-ray Scattering, and Photophysical Studies

Eléna Ishow,[†] André Gourdon,*[,†] Jean-Pierre Launay,[†] Pierre Lecante,[†] Marc Verelst,[†] Claudio Chiorboli,*[,‡] Franco Scandola,[‡] and Carlo-Alberto Bignozzi[‡]

CEMES-CNRS UPR 8011, BP 4347, 29 Rue Jeanne Marvig, 31055 Toulouse, France, and Dipartimento di Chimica, Centro di Reattività e Catalisi CNR, Università di Ferrara, Via L. Borsari 46, 44100 Ferrara, Italy

Received December 17, 1997

The tetranuclear ruthenium complex $\{Ru[(tpphz)Ru(bpy)_2]_3\}^{8+}$, where tpphz is tetrapyrido[3,2-a:2′,3′-c:3″,2″-h:2‴,3‴-j]phenazine, has been synthesized by reaction of $[Ru(tpphz)_3]^{2+}$ with $[Ru(bpy)_2Cl_2]$ and by reaction of $[Ru(bpy)_2(tpphz)]^{2+}$ with $[Ru(DMSO)_4Cl_2]$. The large distance between the chiral centers allows full ^{1}H NMR interpretation despite the mixture of eight stereoisomers. The tetranuclear complex was further characterized by electrospray mass spectrometry and by the wide-angle X-ray scattering technique, which confirmed the starburst geometry. The photophysical properties of the tetranuclear complex in acetonitrile were studied and compared with those of $[Ru(tpphz)_3]^{2+}$ (1×10^{-4} M acidic solution) and $[(bpy)_2Ru(tpphz)Ru(bpy)_2]^{4+}$ model molecules. The tetranuclear complex gives rise to a single emission, attributed to metal-to-ligand charge-transfer states involving peripheral Ru centers and tpphz bridging ligands.

Introduction

The tremendous interest devoted to systems containing multifold chromophoric and electroactive centers arises from the construction of molecular devices based on nanometric and well-defined molecular architectures. Transition-metal dendrimers actually appear as very attractive potential photoconversion and light-harvesting devices due to the rich electrochemical and photophysical properties of the metallic moieties.[1] Contrary to their polymeric counterparts, organometallic dendrimers are characterized by monodisperse size and shape and advantageously permit the formation of assemblies with predetermined functions as antenna effects by judicious and univocal combination of building blocks. These starburst systems can be prepared by two synthetic strategies, the convergent and divergent growth routes. Whereas the latter method must cope with defects within the novel growing generation due to uncomplete reactions, the former, pionnered by Fréchet et al.,[2] can be limited by increasing steric hindrances around the central core. Mathematic growth calculations related to a statistical treatment of these dendritic systems pointed out that a short length of the spacer connecting two successive cascade branches engenders dramatic steric crowdings and extension limitations.[3] Furthermore, the progression toward higher generations of metallic compounds is impeded by purification but, above all, by characterization difficulties, ruling out any ^{1}H NMR technique due to the chirality of each connected metallic center. There is, therefore, a general need for large and well-characterizable motifs in order to better control and check the design of the targeted architectures.

Recently, we reported the first synthesis of the fully aromatic and rigid bridging ligand tpphz (where tpphz is tetrapyrido-[3,2-a:2′,3′-c:3″,2″-h:2‴,3‴-j]phenazine)[4] and of its dinuclear ruthenium and osmium complexes. In these complexes, the distance between the chiral centers is large enough (12.7 Å from X-ray crystallography) to simplify the ^{1}H NMR spectra, allowing full attribution of the proton signals. This was recently confirmed by others for very similar tpphz ruthenium dimers[5] and polymers.[6] Furthermore, the fully rigid nature of this bridging ligand enables a very accurate knowledge of the complex geometry.

In this paper, we present an extension of these rodlike architectures to a D_3 ruthenium tpphz tetranuclear complex ($\{Ru[(tpphz)Ru(bpy)_2]_3\}^{8+}$, Figure 1), synthesized by both divergent and convergent methods.[7] In the absence of single-

[†] CNRS, Toulouse.
[‡] Ferrara University.

(1) See, for example: (a) Serroni, S.; Denti, G.; Campagna, S.; Juris, A.; Ciano, M.; Balzani, V. *Angew. Chem., Int. Ed. Engl.* **1992**, *31*, 1493. (b) Serroni, S.; Denti, G. *Inorg. Chem.* **1992**, *31*, 4251. (c) Denti, G.; Campagna, S.; Serroni, S.; Ciano, M.; Balzani, V. *J. Am. Chem. Soc.* **1992**, *114*, 2944. (d) Serroni, S.; Juris, A.; Campagna, S.; Venturi, M.; Denti, G.; Balzani, V. *J. Am. Chem. Soc.* **1994**, *116*, 9096. (e) Serroni, S.; Denti, G.; Campagna, S.; Ciano, M.; Balzani, V. *J. Chem. Soc., Chem. Commun.* **1991**, 944. (f) Campagna, S.; Denti, G.; Serroni, S.; Juris, A.; Venturi, M.; Ricevuto, V.; Balzani, V. *Chem. Eur. J.* **1995**, *1*, 211. (g) Balzani, V.; Juris, A.; Venturi, M.; Campagna, S.; Serroni, S. *Chem. Rev.* **1996**, *96*, 759. (h) Lehn, J.-M. *Supramolecular Chemistry, Concepts and Perspectives*, VCH: Weinheim, Germany, 1995. (i) Fabbrizzi, L.; Poggi, A. *Transition Metals in Supramolecular Chemistry*; NATO ASI Series 448; Elsevier: Dordrecht, The Netherlands, 1994. (j) Cleary, R. L.; Byrom, K. J.; Bardwell, D. A.; Jefferty, J. C.; Ward, M. D.; Calogero, G.; Armaroli, N.; Flamigni, L.; Barigelletti, F. *Inorg. Chem.* **1997**, *36*, 2601.

(2) (a) Hawker, J. M.; Fréchet, M. J. *J. Chem. Soc., Chem. Commun.* **1990**, 1010. (b) Fréchet, M. J. *Science* **1994**, *263*, 1710. (c) Miller, T. M.; Neeman, T. X.; Zayas, R.; Bair, H. E. *J. Am. Chem. Soc.* **1992**, *114*, 1018.

(3) De Gennes, P. G.; Hervet, H. *J. Phys. Lett.* **1983**, *44*, L-351.

(4) (a) Bolger, J.; Gourdon, A.; Ishow, E.; Launay, J.-P. *J. Chem. Soc., Chem. Commun.* **1995**, 1799. (b) Bolger, J.; Gourdon, A.; Ishow, E.; Launay, J.-P. *Inorg. Chem.* **1996**, *35*, 2937.

(5) MacDonnell, F. M.; Bodige, S. *Inorg. Chem.* **1996**, *35*, 5758.

(6) Knapp, R.; Schott, A.; Rehahn, M. *Macromolecules* **1996**, *29*, 478.

(7) Bodige, S.; Torres, A. S.; Maloney, D. J.; Tate, D.; Kinsel, G. R.; Walker, A. K.; MacDonnell, F. M. *J. Am. Chem. Soc.* **1997**, *119*, 1364 (appeared during the redaction of this paper and presents very complementary results on a phenanthroline analogue of **1**).

S0020-1669(97)01581-4 CCC: $15.00
Published on Web 06/16/1998

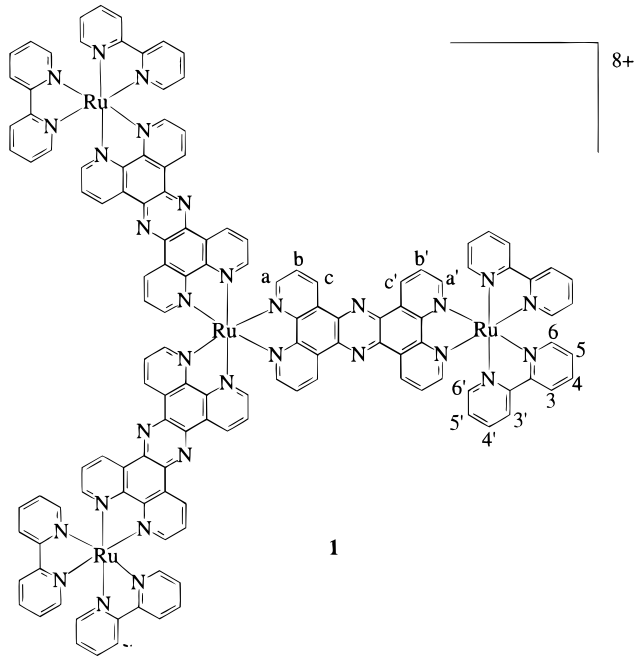

Figure 1. Structure of $\{Ru[(tpphz)Ru(bpy)_2]_3\}^{8+}$.

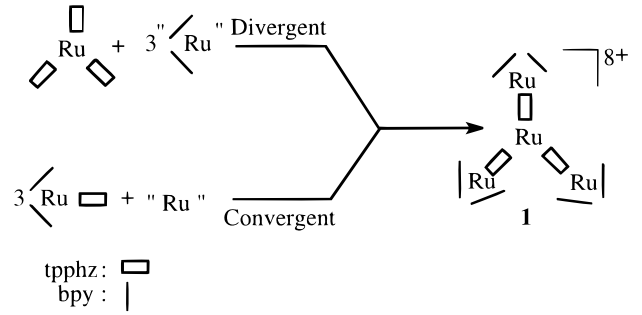

Figure 2. Convergent and divergent routes to **1**. Ru represents $[Ru(DMSO)_4Cl_2]$.

crystal X-ray structure, we introduce the wide-angle X-ray scattering technique (WAXS) as a characterization technique for geometric determination of the polynuclear star-shaped complexes. Given the interest in this class of compounds as artificial light-harvesting devices, this paper contains a full photophysical characterization of the tetranuclear complex, with particular emphasis on the identification of the emitting excited state and on the direction of energy flow within the supramolecular structure.

Results and Discussion

Synthesis. We have prepared the tetranuclear complex **1** by two synthetic routes as shown in Figure 2. The high reactivity of $[Ru(DMSO)_4Cl_2]$ and the length of the tpphz ligand enabled the convergent-type formation of **1** in high yield (up to 91% by ^{1}H NMR integration, see below). Further photophysical experiments have required extensive purifications of the complex, which were performed by exclusion gel chromatography (Sephadex G 25) and gave a total yield of 65%.

The divergent synthesis required the preparation of the poorly soluble precursor $[Ru(tpphz)_3]^{2+}$ by reaction of tpphz with $[Ru(DMSO)_4Cl_2]$ in 65% yield. At this stage, we must stress the absence of any polymerization process despite the two chelating parts of the tpphz ligand. This feature was actually checked by WAXS on raw $[Ru(tpphz)_3]^{2+}$, which showed no signal corresponding to a Ru−tpphz−Ru distance. Growth toward **1** was accomplished by reacting 1 equiv of $[Ru(tpphz)_3]^{2+}$ with 3 equiv of $[Ru(bpy)_2Cl_2]$ in 33% yield. This latter yield contrasts with the former reported for the convergent method and is probably related to the very poor solubility of $[Ru(tpphz)_3]^{2+}$.

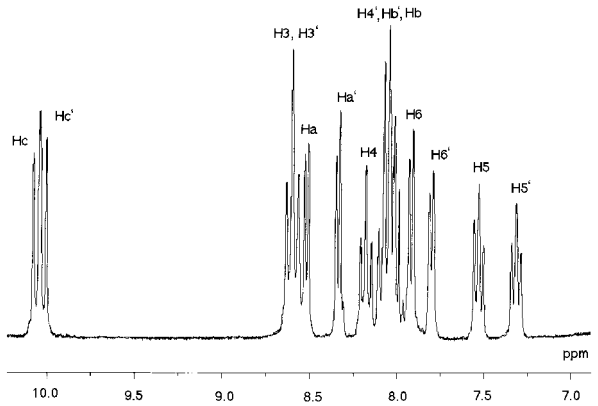

Figure 3. 250-MHz ^{1}H NMR spectrum of **1** in acetonitrile-d_3. The attribution refers to the labeling in Figure 1.

It must be emphasized that both synthetic methods allow full ^{1}H NMR monitoring of the complexation reaction, as the signals corresponding to the Hc′ protons of **1** and of the other two mononuclear complexes appear in distinct low-field spectral regions.

^{1}H NMR. As expected on the basis of previous results,[4] and contrary to most multinuclear complexes for which full ^{1}H NMR characterization requires enantiomeric resolutions,[8] the proton signals of the tetranuclear complex were unambiguously assigned. This simple magnetic pattern (Figure 3) actually originates from the large distance between the core and the peripheral ruthenium centers (12.7 Å) and between peripheral ligands (minimum 15.4 Å). At these distances, each chiral center is not influenced by its neighbors, so that the ^{1}H NMR spectra of all eight stereoisomers exactly superimpose.[7]

This spectrum obviously confirms the expected D_3 symmetry of **1**. In contrast with the phenanthroline analogue recorded in the same frequency conditions,[7] the eight magnetically unequivalent protons belonging to the same ancillary bipyridine are well distinguishable. Rotation of pyridyl units around the 2,2′ single bond is effectively allowed by the more flexible bipyridine in order to better accommodate with the steric repulsions. This novel spatial arrangement is certainly responsible for the slightly more deshielded Hb′ (8.06 ppm) close to $[Ru(bpy)_2]^{2+}$ extremities than the Hb protons (8.02 ppm) close to the ruthenium core due to anisotropic magnetic effects from the pyridine cycle. This observation is in total agreement with the data reported for the tpphz-based mononuclear $[Ru(bpy)_2(tpphz)]^{2+}$ complex, where Hb′ (close to the metal) and Hb (uncomplexed part) were found at 7.89 and 7.83 ppm, whereas again opposite behaviors were described for the phen analogue of **1**, where Hb′ and Hb resonated at respectively 7.87 and 7.96 ppm.

Mass Spectroscopy. The tetranuclear complex **1** was further characterized by electrospray mass spectrometry in CH_3CN/H_2O (Figure 4). Peaks of perfectly resolved state of charge were found at *m/z* 1073 ($[M - 3PF_6]^{3+}$), 767.7 ($[M - 4PF_6]^{4+}$), 586.1 ($[M - 5PF_6]^{5+}$), and 464.1 ($[M - 6PF_6]^{6+}$). Some peaks

(8) (a) Tzalis, D.; Tor, Y. *J. Am. Chem. Soc.* **1997**, *119*, 852. (b) Fletcher, N. C.; Keene, F. R.; Viebrock, H.; von Zelewsky, A. *Inorg. Chem.* **1997**, *36*, 1113. (c) Kelso, L. S.; Reitsma, D. A.; Keene, F. R. *Inorg. Chem.* **1996**, *35*, 5144. (d) Rutherford, T. J.; Van Gije, O.; Kirsch-De Mesmaeker, A.; Kenne F. R. *Inorg. Chem.* **1997**, *36*, 4465.

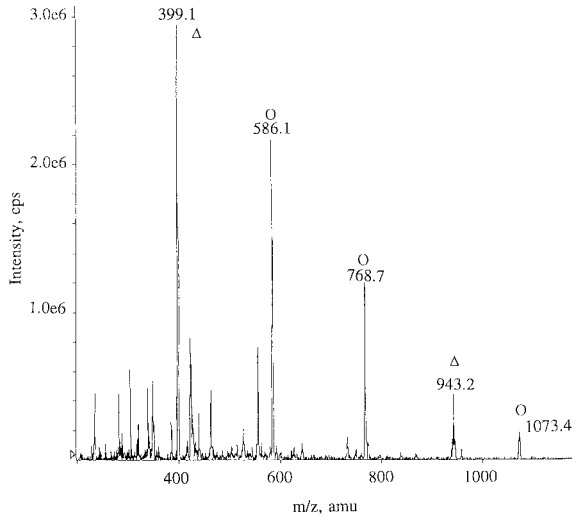

Figure 4. ES-MS spectrum of **1**. $\{Ru[(tpphz)Ru(bpy)_2]_3\}^{8+}$, ○; $[(tpphz)Ru(bpy)_2]^{2+}$, △.

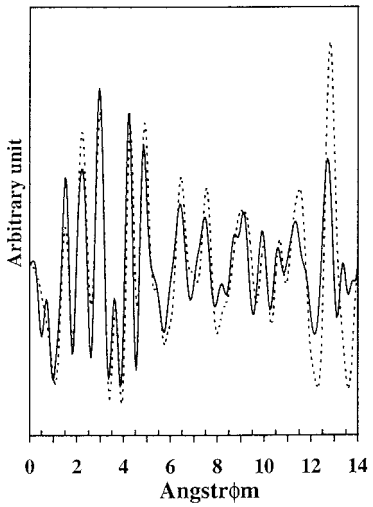

Figure 5. Experimental RDF for **1** (plain line) compared with calculated RDF from the theoretical model (dotted line).

were also detected at *m*/*z* 943.2 ($[M' - PF_6]^+$) and 399.1 ($[M' - 2PF_6]^{2+}$) and were attributed to the $[(tpphz)Ru(bpy)_2]^{2+}$ moiety. This species is not an impurity, as shown by NMR spectroscopy, but results from fragmentation of the tetranuclear species even at low accelerating voltage (60 V). In contrast with 1,4,5,8,9,12-hexaazatriphenylene (HAT) heptanuclear ruthenium complexes,[9] we have not observed the formation of POF_4^-, $PO_2F_2^-$, and phosphates resulting from the hydrolysis of PF_6^-.

WAXS. Figure 5 shows the experimental reduced radial distribution function (RDF) obtained from Fourier transform of the scattering pattern compared with the theoretical one calculated from the model. Roughly, an RDF can be considered as a histogram of ordered distances in the molecule weighted by two factors: the number of electrons engaged in this distance and the multiplicity of the distance. Thus, an intense RDF peak indicates a distance between two heavy atoms and/or a very frequent distance.

The fitting agreement between the experience and the model is nearly perfect, proving indisputably that the star tetranuclear model is the right one. The only significant discrepancy is a slight shift of the intense peak centered at 12.7 Å in the experimental RDF and at 12.85 Å in the model. That peak is mostly related to Ru−Ru atom pair correlation, which is slightly overevaluated in the model, probably because the exact geometry of the quinoxaline unit is not perfectly reproduced by the universal force field[10] used in this model. It can be emphasized that this metal−metal distance obtained from experimental RDF corresponds exactly to the one observed in the X-ray structure.[4a] Beyond 13 Å, the goodness of fit decreases gradually (not shown). However, for such a long pair correlation, intermolecular interactions which are not taken into account by a single-molecule model become nonnegligible.

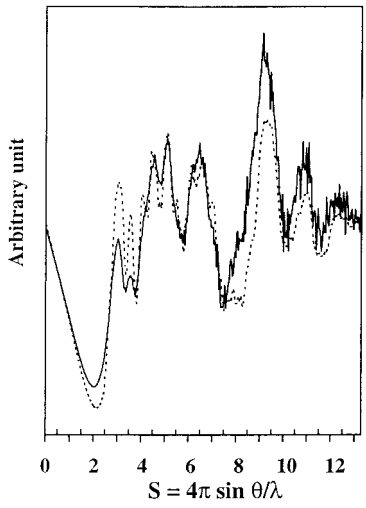

Figure 6. Experimental reduced intensity for **1** (plain line) compared with the theoretical one (dotted line).

If RDF analysis in the direct space is very convenient, then the fitting agreement is probably better appreciated on reduced intensity in the reciprocal space. Indeed, fitting on reduced intensities allows more direct comparison of the experimental scattering pattern with the theoretical one without any mathematical transformation. Figure 6 shows that the fitting agreement on reduced intensity is also good and confirms the starburst tetranuclear geometry depicted Figure 1.

Electrochemistry. The electrochemical properties of **1** have been studied in acetonitrile and DMF. As for the mono- and dinuclear tpphz complexes, the reductions are not well-behaved in acetonitrile, probably due to adsorption of the reduced species on the working electrode. To minimize this problem, the reduction processes have been studied in DMF using a carbon disk as working electrode, whereas the oxidation processes have been studied in acetonitrile, which permits higher applied potentials (Table 1).[11]

Cyclic voltammograms of **1** show two reversible metal-based oxidations (in ratio 3:1) and three reversible ligand-based reductions. The first oxidation potential, at 1.35 V, is very close to the $[Ru(bpy)_3]^{2+}$, $[Ru(bpy)_2(tpphz)]^{2+}$, and $[Ru(bpy)_2(tpphz)$-$Ru(bpy)_2]^{4+}$ ones. We have shown for these two tpphz complexes[4b] that the HOMO has little contribution from the phenazine part, which means that the tpphz ligand, despite its strong π-accepting character, exerted almost no influence on the ruthenium oxidation potential. This three-electron oxidation wave can, therefore, be attributed without any ambiguity to the simultaneous oxidations of the three terminal ruthenium centers.

(9) Moucheron, C.; Kirsch-De Mesmaeker, A.; Dupont-Gervais, A.; Van Dorsselaer, A. *J. Am. Chem. Soc.* **1996**, *118*, 12834.

(10) Rappé, A. K.; Casewit, C. J.; Colwell, K. S.; Goddard, W. A.; Skiff, W. M. *J. Am. Chem. Soc.* **1992**, *114*, 10024.

(11) Due to the high insolubility of the mononuclear $[Ru(tpphz)_3]^{2+}$ in common solvents, its electrochemistry was not studied.

Table 1. Half-Wave Potentials E(V) for the Oxidation, E_{ox}, and the Reduction, E_{red} of the Complexes[a,b]

species	E_{ox1}	E_{ox2}	E_{red1}	E_{red2}	E_{red3}
$[Ru(bpy)_3]^{2+}$ [c]	1.27		−1.31	−1.50	−1.77
$[Ru(bpy)_2(tpphz)]^{2+}$ [c]	1.33		−0.87	−1.33	−1.51
$[Ru(bpy)_2(tpphz)Ru(bpy)_2]^{4+}$ [c]	1.34 (2e$^-$)		−0.71	−1.31 (2e$^-$)	−1.51 (2e$^-$)
$\{Ru[(tpphz)Ru(bpy)_2]_3\}^{8+}$	1.35 (3e$^-$)	1.50	−0.74 (3e$^-$)	−1.30 (3e$^-$)	−1.48 (3e$^-$)

[a] Unless otherwise noted, the oxidation potentials are given vs SCE in CH_3CN, and the reduction potentials are given vs SCE in DMF; in both cases, the supporting electrolyte is 0.1 M NBu_4PF_6 at room temperature; scan speed, 0.1 V s^{-1}; internal reference $Fc/Fc^+ = 0.48$ V. [b] All complexes are PF_6 salts. [c] From ref 4b.

Table 2. Spectroscopic and Photophysical Properties

	absorption (MLCT), 298 K[a]		emission			
			298 K[a]			77 K[b]
complexes	λ_{max} (nm)	ϵ, (M^{-1} cm^{-1})	λ_{max} (nm)[c]	τ, (ns)[d]	Φ ($\times 10^{-3}$)	λ_{max} (nm)[c]
$[(bpy)_2Ru(tpphz)Ru(bpy)_2]^{4+}$	442	36 950	690	90	5.6	586
$[Ru(tpphz)_3]^{2+}$ [e]	432	20 500	715	80	5.5	590
$\{[Ru(tpphz)_3][Ru(bpy)_2]_3\}^{8+}$	440	71 600	745	50	2.5	594

[a] Solvent, acetonitrile. [b] Matrix, EtOH/MeOH 4:1. [c] From corrected emission spectra. [d] From time-resolved single-photon counting. [e] With 10^{-4} M trifluoromethanesulfonic acid.

This confirms that, as in the dinuclear complex, the large intermetallic $Ru_{terminal}-Ru_{terminal}$ distances (calculated 22 Å), rule out any important Coulombic interaction between the three outer metallic centers. The second oxidation wave at 1.50 V involves one electron and is attributed to the central ruthenium atom. Once again, and for the same reasons, this potential is relatively low for a Ru(II) atom surrounded by three π-accepting tpphz and three triply charged metal centers.

The reduction part shows three successive three-electron processes. By analogy with the mono- and dinuclear tpphz ruthenium complexes, the first reduction wave can be attributed to the simultaneous reductions of the three tpphz bridging ligands. These complexes are significantly better electron acceptors than $[Ru(bpy)_3]^{2+}$ by 0.5−0.6 V, their LUMO being mainly localized on the phenazine part. As for the oxidation of the terminal ruthenium(II) ions, the simultaneous reduction of the three tpphz shows that these three sites are not interacting. This behavior is also observed for the second and third reductions: the second three-electron reduction process (−1.30 V) can be attributed to the simultaneous reductions of one 2,2′-bipyridine of each terminal ruthenium at a potential very close to that of the first reduction of $[Ru(bpy)_3]^{2+}$ (−1.31 V) to give the species $\{Ru[(tpphz^{\bullet-})Ru(bpy^{\bullet-})(bpy)]_3\}^{2+}$. The third reduction, at −1.48 V, involves three electrons and can be attributed to the simultaneous reduction of the second 2,2′-bipyridine of each terminal ruthenium center to give the anionic species $\{Ru[(tpphz^{\bullet-})Ru(bpy^{\bullet-})(bpy^{\bullet-})]_3\}^{-}$. This potential is comparable to the second reduction process of $[Ru(bpy)_3]^{2+}$, generating $[Ru(bpy)(bpy^{\bullet-})(bpy^{\bullet-})]$ (−1.50 V). These reduction processes are very similar to those of the dinuclear $[(bpy)_2Ru(tpphz)Ru(bpy)_2]^{4+}$, which prompted us to use this dinuclear complex as a reliable model for the study of the photophysical properties of the tetranuclear complex.

Absorption Spectra. The absorption spectrum of the $\{Ru[(tpphz)Ru(bpy)_2]_3\}^{8+}$ tetranuclear complex in acetonitrile solution is presented in Figure 7. For comparison purposes, the absorption spectra of $[Ru(tpphz)_3]^{2+}$ and $[(bpy)_2Ru(tpphz)Ru(bpy)_2]^{4+}$ are also reported. These consist of three distinct spectral regions. The visible region ($\lambda > 400$ nm) contains the typical MLCT transitions of Ru(II) polypyridine complexes. The bands are broad, centered at about 450 nm, without any appreciable resolution of MLCT transitions involving different polypyridine ligands and/or different metal centers. This is not unexpected since, as discussed in detail elsewhere,[4b,12] the MOs involved in this optical absorption are largely bpy-centered in character. As expected, the molar absorptivities in this spectral region (Table 2) scale approximately as the total number of Ru(II)($d\pi$)−bpy(π^*) MLCT transitions expected for each complex (nuclearity × 3). The bands in the narrow 350−400-nm spectral region correspond to n−π^* and $\pi-\pi^*$ transitions localized on the tpphz ligand. They exhibit a characteristic sharp structure, and their intensity clearly scales again as the number of electronically decoupled tpphz ligands present in the complex. The region at $\lambda < 350$ nm contains very intense overlapping $\pi-\pi^*$ transitions of both bpy and tpphz ligands.

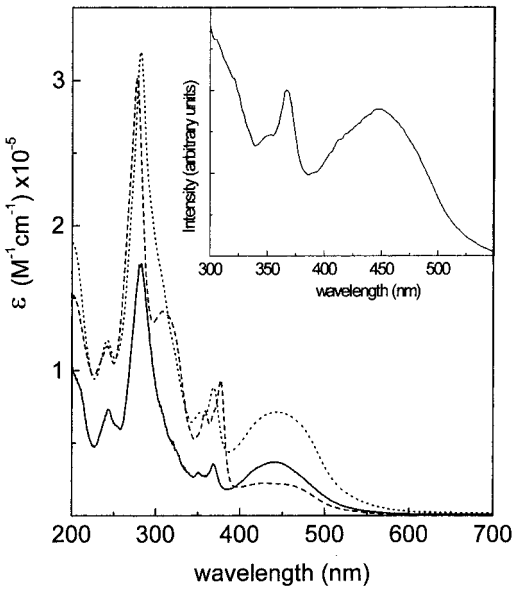

Figure 7. Absorption spectra in acetonitrile solution: $[(bpy)_2Ru(tpphz)Ru(bpy)_2]^{4+}$ (—), $\{[Ru[(tpphz)Ru(bpy)_2]_3\}^{8+}$ (•••), and $[Ru(tpphz)_3]^{2+}$ in 1×10^{-4} M CF_3SO_3H (- - -). Inset: excitation spectrum of $\{Ru[(tpphz)Ru(bpy)_2]_3\}^{8+}$ in acetonitrile solution (emission wavelength, 745 nm).

Photophysics of Model Compounds. As for many other ligand-bridged polynuclear complexes, it is convenient to consider $\{Ru[(tpphz)Ru(bpy)_2]_3\}^{8+}$ as a covalently linked supramolecular system, made up of molecular components

(12) Chiorboli, C.; Bignozzi, C. A.; Scandola, F.; Ishow, E.; Gourdon, A.; Launay, J.-P., manuscript in preparation.

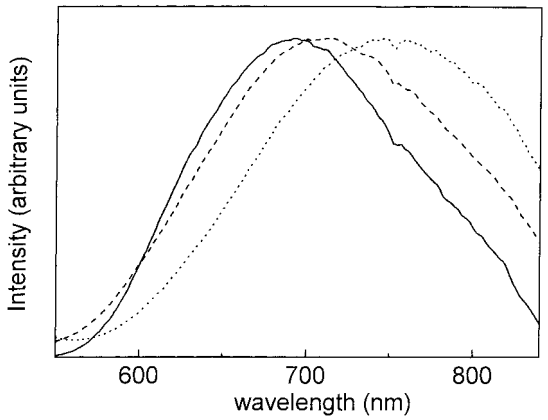

Figure 8. Room-temperature emission spectra in acetonitrile solution: $[(bpy)_2Ru(tpphz)Ru(bpy)_2]^{4+}$ (—), $\{Ru[(tpphz)Ru(bpy)_2]_3\}^{8+}$ (••), and $[Ru(tpphz)_3]^{2+}$ in 1×10^{-4} M CF_3SO_3H (- - -). The spectra are corrected for instrumental response.

characterized by individual spectroscopic and photophysical properties. In principle, such individual properties can be inferred from the behavior of suitable model systems. In this case, however, the identification of suitable molecular models is a nontrivial problem. Intuitively, $[Ru(tpphz)_3]^{2+}$ and $[Ru(bpy)_2(tpphz)]^{2+}$ could be considered as models for, respectively, the central unit and the three peripheral ones. In fact, it is known that $[Ru(bpy)_2(tpphz)]^{2+}$ is quite sensitive to covalent interactions, such as protonation or metalation, at the free end of the tpphz ligand.[12] Such interactions result, e.g., in a substantial red shift and lifetime shortening of the MLCT emission. The same qualitative behavior is expected to be followed by $[Ru(tpphz)_3]^{2+}$. Thus, a more reasonable model for the three peripheral units could be the binuclear $[(bpy)_2Ru(tpphz)Ru(bpy)_2]^{4+}$ complex. For the central unit, a protonated form of $[Ru(tpphz)_3]^{2+}$ (obtained by dissolution of the complex in acetonitrile containing 1×10^{-4} M trifluoromethanesulfonic acid, presumably $[Ru(tpphz)_3]^{2+}\cdot 3H^+$) could be used as a model.

These two model compounds exhibit very similar photophysical behaviors. Their emissions have very similar lifetimes, quantum yields, and maximum wavelengths (Figure 8 and Table 2). The onset of the MLCT emission, indicating the expected MLCT 0−0 energy of the molecular component, is practically the same for the two models (Figure 8). The ratio of quantum yield and lifetime gives radiative rate constant values of ca. 5×10^4 s^{-1}, quite typical for MLCT emission of Ru(II) polypyridine complexes. For the $[(bpy)_2Ru(tpphz)Ru(bpy)_2]^{4+}$ model, the MLCT emitting state could, in principle, involve either the bpy or the tpphz ligands. Based on the red shift observed with respect to $[Ru(bpy)_2(tpphz)]^{2+}$, it is safe to conclude that the emission involves the tpphz bridging ligand. Independent evidence for this assignment comes from the electrochemistry of the model,[4] clearly indicating that the lowest-energy reduction takes place at the tpphz, rather than bpy, ligands. As discussed in detail elsewhere,[4,12] in the emitting MLCT state at room temperature, the excited electron resides in a MO largely centered on the phenazine region of the tpphz ligand.

The very large blue shift observed when the emission of both models is measured at 77 K (Table 2) is, as discussed elsewhere,[12] a solvent-rigidochromic effect. The intraligand electron-transfer process leading from the MLCT state involving the bpy-like portion of tpphz to the room-temperature emitting MLCT state, involving the phenazine part of tpphz, requires solvent repolarization and is practically blocked in the low-temperature rigid glass.

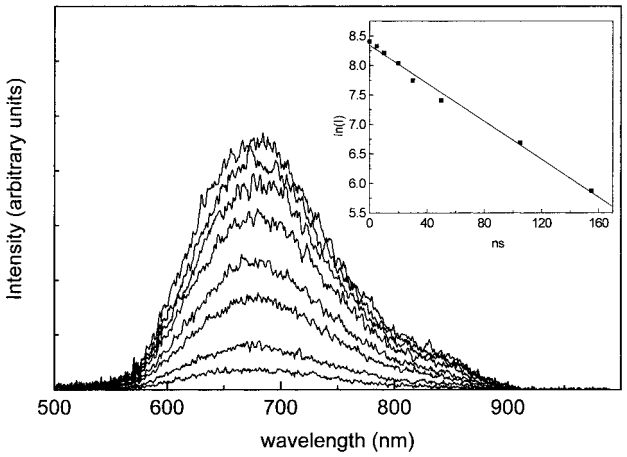

Figure 9. Time-resolved emission spectra of $\{Ru[(tpphz)Ru(bpy)_2]_3\}^{8+}$ in acetonitrile solution (298 K; $\lambda_{exc} = 532$ nm; gate width, 5 nm; delay times, 0, 5, 10, 20, 30, 50, 105, 155 ns). Inset: first-order plot of the emission decay ($t = 55 \pm 5$ ns).

Photophysics of the Tetranuclear Complex. The emission of the tetranuclear $\{Ru[(tpphz)Ru(bpy)_2]_3\}^{8+}$ complex (Figure 8) appears to be, from all experimental viewpoints, a single MLCT emission. It decays with constant profile and single-exponential kinetics (Figure 9). The lifetime and quantum yield are both somewhat smaller than those of the two putative models, yielding a value of 5×10^4 s^{-1} for the radiative rate constant. As shown by the great similarities between excitation and absorption spectra (Figure 7), the emission efficiency is appreciably constant as a function of excitation energy throughout the whole UV−visible spectral region. This suggests that the excitation energy deposited by light in any part of the tetranuclear complex is efficiently conveyed to a single metal-containing fragment by means of fast intercomponent processes, which gives rise to the observed MLCT emission.

As already discussed for the $[(bpy)_2Ru(tpphz)Ru(bpy)_2]^{4+}$ model, the MLCT emission of the tetranuclear complex is not expected to involve the bpy ligands. As a matter of fact, the electrochemistry of $\{Ru[(tpphz)Ru(bpy)_2]_3\}^{8+}$ (Table 1) is very clear in indicating that the lowest-energy reduction takes place at tpphz (−0.74 V vs SCE, $3e^-$) rather than at bpy ligands (−1.30 V vs SCE, $3e^-$; −1.48 V vs SCE, $3e^-$). Thus, the excited electron resides on the bridging tpphz ligand, and the identification of the emitting unit reduces to the identification of the ruthenium atom (central or peripheral) being involved in the MLCT excited state. Photophysical results alone do not allow full resolution of this dilemna. In fact, the emission is not truly coincident with that of any of the two putative models (Figure 8 and Table 2). Again, the most useful tool is represented by electrochemistry (Table 1), which clearly shows that the first oxidation in the tetranuclear complex takes place at the peripheral ruthenium ions (+1.35 V vs SCE, $3e^-$) rather than at the central one (+1.50 V vs SCE, $1e^-$). On this basis, the emitting state can be identified as an MLCT state from peripheral Ru to tpphz. As far as the center-to-periphery energy flow within the tetranuclear complex is concerned, $\{Ru[(tpphz)Ru(bpy)_2]_3\}^{8+}$ behaves in the same way as the other homotetranuclear complexes of the type $\{Ru[(BL)Ru(bpy)_2]_3\}^{8+}$ (BL = bridging ligand).[1,14]

(13) Balzani, V.; Scandola, F. *Supramolecular Photochemistry*; Horwood: Chichester, U.K., 1991.
(14) Denti, G.; Campagna, S.; Sabatino L.; Serroni, S.; Ciano, M.; Balzani V. *Inorg. Chem.* **1990**, *29*, 4750.

In supramolecular antenna systems, migration of the excitation energy between central and peripheral units is normally assumed to proceed via intercomponent energy-transfer processes. In $\{Ru[(tpphz)Ru(bpy)_2]_3\}^{8+}$, given the nature of the involved excited state, an alternative viewpoint can also be taken. In both MLCT excited states, the excited electron is placed on the bridging ligand and, as discussed previously for analogous binuclear complexes,[4,12] presumably in a MO substantially localized on the central phenazine-like part. Consequently, the difference between the two MLCT states comes from the localization of the "hole" (3+ oxidation state), namely either on the central or on a peripheral Ru atom. Therefore, what is formally considered as an "energy transfer" from the central unit to the peripheral ones is in reality a *metal-to-metal* (peripheral Ru to central Ru) *electron* transfer. It is commonly considered that small-driving-force electron-transfer processes should be suppressed on going from room-temperature solutions to low-temperature rigid glasses. In the present case, such a check is complicated by the peculiar rigidochromic behavior of tpphz-bridged Ru complexes. Similarly to what happens for the analogous binuclear complex, the emission at 77 K is very strongly blue shifted relative to that at room temperature (Table 2) and becomes very close to the $[Ru(bpy)_3]^{2+}$ emission. This is consistent with the assumption that MLCT states involving the metal-bound bpy-like portions of tpphz cannot relax in this medium by intraligand electron transfer to the central phenazine-like portion of tpphz.

Conclusions

In summary, we have shown that the use of the fully aromatic long and rigid tpphz bridging ligand allowed the full ^{1}H NMR characterization of the tetranuclear ruthenium complex $\{Ru[(tpphz)Ru(bpy)_2]_3\}^{8+}$. Moreover, ^{1}H NMR investigations appeared as an efficient tool for monitoring the complexation of the noncoordinated tpphz parts of the mononuclear complexes yielding the tetranuclear species. Following the same building-block stategy as developped for the dinuclear tpphz complexes, further extensions toward higher tpphz dendrimer generations could also take advantage of these peculiar and reliable spectroscopic features in order to check the completion of each novel branch connection. The photophysical study has shown that starburst structures based on long, rigid tpphz bridges maintain energy-transfer capabilities comparable to those of analogues containing shorter bridges. Thus, tpphz appears as a suitable bridging ligand for the construction of artificial antenna systems. The possibility of controlling the energy flow direction in such systems through well-chosen heterometallic substitutions is currently being explored.

Experimental Section

Materials. tpphz and $[Ru(bpy)_2(tpphz)](PF_6)_2$ were synthesized according to ref 4. $[Ru(DMSO)_4Cl_2]$ was prepared according to ref 15. NBu_4PF_6 was recrystallized several times from ethanol and dried for 24 h at 140 °C under vacuum. All other solvents and reagents used were at least reagent grade quality and were used without further purification. All the solvents used for spectrophotometric and photophysical measurements were of spectroscopic grade.

Methods and Instrumentation. UV−vis−near-IR spectra were taken on a Shimadzu UV-3100 spectrophotometer. 1D and 2D ^{1}H NMR spectra were recorded on Bruker WF-250 and Bruker AMX-400 spectrometers and processed with the program SwaN-MR.[16] Chemical shifts were measured with reference to the residual solvent signals. Electrochemical measurements were performed on an Electromat 2000 system. Cyclic voltammograms were obtained using a platinum working electrode, a platinum auxiliary electrode, and a saturated potassium chloride calomel reference electrode (Tacussel). Linear and differential pulsed voltammetry were done using a platinum rotating disk electrode. At the end of each experiment, ferrocene was added as an internal standard, with $Fc/Fc^+ = 480$ mV vs SCE. The potentials were then automatically corrected for uncompensated cell resistance.[17] FAB mass spectra were recorded on a Nermag R10-R10 spectrometer using 3-nitrobenzyl alcohol as a matrix. ES mass spectra were recorded on a Perkin-Elmer SCIEX equipped with a LCMS System API 100.

WAXS. A small amount of the powder was sealed in a 1.5-mm-diameter Lindemann glass capillary. Measurements of the X-ray intensity scattered by the sample irradiated with graphite-monochromatized molybdenum Kα (0.710 69 Å) radiation were performed using a dedicated two-axis diffractometer. Duration of a data collection was typically 60 h for a set of 457 values collected at room temperature in the range $0° < \theta < 65°$ for equidistant s values ($s = 4\pi(\sin\theta/\lambda)$; $\Delta s = 0.035$ Å^{-1}). To separate the intensity related to the sample from other contributions, scattering patterns from air and empty capillary were also collected under the same conditions. The raw intensity was then corrected for air and capillary attenuated by sample absorption. Polarization and self-absorption corrections were also applied. Data were reduced using previously described procedures[18] in order to extract the structure-related component of WAXS, the so-called reduced intensity function $i(s)$, which was then Fourier transformed to allow for radial distribution function (RDF) analysis. To further investigate the structure, a model was built using the CERIUS2 program[19] and universal force field (UFF).[20] A molecular mechanics procedure was applied for energy minimization. UFF parameters were used without any change except for the free nitrogen ruthenium distance, which was adjusted to 2.06 Å, as usually encountered in ruthenium bipyridine units. The refined model was then used for the computation of theoretical functions for intensity and radial distribution via Debye's formula.[21]

Photophysics. Steady-state luminescence studies were performed using a Perkin-Elmer MPF 44E spectrofluorometer. For 77 K emission spectra, an Oxford DN704 cryostat equipped with an Oxford DTC-2 temperature controller was used. Emission lifetimes were measured using a PRA system 3000 time-correlated single-photon counting apparatus equipped with a Norland model 5000 MCA card and a hydrogen discharge pulsing lamp (50 kHz, halfwidth 2 ns). The decays were analyzed by means of Edinburgh FLA900 software. Alternatively, an Applied Photophysics laser flash photolysis apparatus was used, with a Continuum model Surelite II Nd:YAG laser (halfwidth 4−6 ns), frequency doubled (532 nm, 330 mJ) or tripled (355 nm, 160 mJ). The photomultiplier (Hamamatsu R928) signal was processed by means of a LeCroy 9360 (600 MHz, 5 Gs/s) digital oscilloscope.

Time-resolved emission spectra were collected using an optical multichannel analyzer, PARC OMA III, equipped with a spectrograph and a gated image intensified diode-array detector (PARC, model 1455). The detector has a minimum gate windows of 5 ns, with an adjustable delay from 0 to 256 ns (PARC, model 1302 fast pulser).

(15) Evans, P.; Spencer, A.; Wilkinson, G. *J. Chem. Soc., Dalton Trans* **1973**, 204.
(16) Balacco, G. *J. Chem. Inf. Comput. Sci.* **1994**, *34*, 1235.
(17) Cassoux, P.; Dartiguepeyron, R.; Fabre, P.-L.; De Montauzon, D. *Electrochim. Acta* **1985**, *30*, 1485.
(18) See, for example: (a) Mosset, A.; Lecante, P.; Galy, J. *Philos. Mag. B* **1982**, *46*, 137. (b) Burian, A.; Lecante, P.; Mosset A.; Galy, J. *J. Non-Cryst. Solids* **1987**, *90*, 633. (c) Laberty, C; Verelst, M.; Lecante, P.; Mosset, A.; Alphonse, P.; Rousset, A. *J. Solid-State Chem.* **1997**, *129*, 271. (d) Verelst, M.; Sommier, L.; Lecante, P.; Mosset, A.; Kahn, O. *Chem. Mater.* **1998**, *10*, 980.
(19) CERIUS2 molecular simulation program is supplied by MSI technologies and was used on an Indy Silicon Graphics workstation.
(20) See, for example: Rappe, A.; Colwell, K.; Casewit, C. *Inorg. Chem.* **1993**, *32*, 3438.
(21) $i_D(s) = 2\sum_{i=1}^{N-1}\sum_{j=i+1}^{N} f_i(s)f_j(s)[\sin(sr_{ij})/sr_{ij}] \exp(-b_{ij}s^2)$, where N is the total number of atoms in the model, f_i the atomic scattering factor for atom i, r_{ij} the distance between atoms i and j, and b_{ij} a dispersion factor affecting the $i-j$ interaction. See: Debye, P. *Ann. Phys. (Leipzig)* **1915**, *46*, 809.

Luminescence quantum yields were measured in optically diluted solutions, using $[Ru(bpy)_3]^{2+}$ in oxygen-free acetonitrile ($\Phi = 0.06$) as reference emitter. Estimated experimental errors in the reported data are as follows: absorption and emission maxima, ±2 nm, emission lifetimes and emission quantum yields, ±10%.

Deaeration of the solutions was carried out by multiple freeze−pump−thaw cycles.

Complex Syntheses. (a) $[Ru(tpphz)_3](PF_6)_2$. A suspension of $[Ru(DMSO)_4Cl_2]$ (61 mg, 0.127 mmol) and tpphz (150 mg, 0.397 mmol) in ethylene glycol (20 mL) was thoroughly deoxygenated by argon bubbling. The mixture was then heated in an oil bath at 170 °C until full dissolution of the reactants. The dark red solution was then stirred for 30 mn at 120 °C. After cooling of the solution to room temperature, addition of an aqueous solution of NH_4PF_6 (30 mL) yielded a red precipitate which was dissolved in an acetonitrile/trifluoroacetic acid mixture. Addition of water, followed by concentration under vacuum, gave 128 mg of pure complex (yield 65%). ^{1}H NMR (CD_3-CN/trifluoroacetic acid-*d*), δ, ppm (number of protons, multiplicity, attribution, *J*, *J*′): 10.38 (6H, dd, Hc′, 8.5 Hz, 1.4 Hz); 10.07 (6H, dd, Hc, 8.3 Hz, 1.2 Hz); 9.40 (6H, dd, Ha′, 5.2 Hz, 1.4 Hz); 8.53−8.47 (m, 12H, Hb′, Ha); 8.03 (d, 6H, Hb, 8.5 Hz, 5.3 Hz). MS [FAB (NBA), *m*/*z*]: 1399 ($[M - PF_6 + H]^+$), 1254 ($[M - 2PF_6 + H]^+$), 627 ($[M - 2PF_6]^{2+}$). Anal. Calcd for $C_{72}H_{36}N_{18}F_2P_{12}Ru\cdot{}^3/_4CF_3CO_2H$, $14H_2O$: C, 46.91; H 2.80; N 13.39. Found: C, 46.71; H 3.46; N 13.31.

(b)$\{$Ru[(tpphz)Ru(bpy)$_2$]$_3\}$(PF$_6$)$_8$. (i) Convergent Synthesis. Twenty milligrams (0.041 mmol) of $[Ru(DMSO)_4Cl_2]$ was suspended with 150 mg (0.127 mmol) of $[Ru(bpy)_2(tpphz)](PF_6)_2$ in thoroughly deoxygenated ethylene glycol (10 mL). The mixture was then submitted to the same experimental procedure as for the $[Ru(tpphz)_3](PF_6)_2$. Addition of ^{n}Bu$_4$NBr to an acetonitrile solution of the hexafluorophosphate salt gave the bromide salt, which was purified by exclusion gel chromatography (Sephadex G-25, eluent. 0.1 M NaCl). The red band was collected and concentrated under vacuum. Addition of NH_4PF_6 gave the tetranuclear complex as its hexafluorophosphate salt. Yield: 97 mg (65%).

(ii) Divergent Synthesis. A solution of $[Ru(bpy)_2Cl_2]$ (66.7 mg (0.128 mmol) and $AgCF_3SO_3$ (99 mg, 0.384 mmol) in MeOH (2 mL) was stirred for 1 h. To the centrifugated and filtered supernatant solution were added 60 mg (0.039 mmol) of $[Ru(tpphz)_3](PF_6)_2$ and 10 mL of ethylene glycol. The mixture was deoxygenated and heated to reflux for 3 days under argon. After cooling at room temperature, the complex was precipitated through addition of 15 mL of aqueous NH_4PF_6. The tetranuclear compound was purified following the same procedure as for the convergent synthesis. Yield: 47 mg (33%). ^{1}H NMR (CD_3CN/trifluoroacetic acid-*d*), δ, ppm (number of protons, multiplicity, attribution, *J*, *J*′): 10.06 (6H, d, Hc, 8.9 Hz); 10.02 (6H, d, Hc′, 8.2 Hz); 8.80 (6H, d, H3, 8.6 Hz); 8.62 (6H, d, H3′, 8.6 Hz); 8.51 (6H, d, Ha, 4.8 Hz); 8.34 (6H, d, Ha′, 4.4 Hz); 8.18 (6H, td, H4′, 8.0 Hz, 1.1 Hz); 8.10−7.99 (18H, m, H4, Hb′, Hb); 7.92 (6H, d, H6, 5.4 Hz); 7.80 (6H, d, H6′, 5.5 Hz); 7.57 (6H, dd, H5, 6.7 Hz, 6.3 Hz); 7.31 (6H, ddd, H5′, 7.0 Hz, 6.2 Hz, 1.1 Hz). MS [ESMS (CH_3CN), *m*/*z*]: 1073 ($[M - 3PF_6]^{3+}$), 768.7 ($[M - 4PF_6]^{4+}$), 686.1 ($[M - 5PF_6]^{5+}$), 464.1 ($[M - 6PF_6]^{6+}$). Anal. Calcd for the bromide salt $C_{132}H_{84}N_{30}Br_8Ru_4\cdot 14H_2O$: C, 46.82; H, 3.33; N, 12.41. Found: C, 46.77; H, 3.62; N, 12.40.

Acknowledgment. The financial assistance of CNRS (France), MURST and CNR (Italy), and EEC (CHRXCT-94-0538) is gratefully acknowledged. Thanks are also expressed to G. Balacco (Menarini Industrie) for a copy of SwaN-MR and to S. Richelme for ES-MS experiments.

IC9715815